Substrate effects in the magneto-optical second-harmonic generation from first principles: Fe/Cu(001)

Torsten Andersen[1,*] and W. Hübner[1,2,†]
[1]*Max-Planck-Institut für Mikrostrukturphysik, Weinberg 2, D-06120 Halle/Saale, Germany*
[2]*Institut für Theoretische Physik, Karl-Franzens-Universität Graz, Universitätsplatz 5, A-8010 Graz, Austria*
(Received 23 October 2001; published 22 April 2002)

We compute the nonlinear optical response of an Fe monolayer placed on top of 1 to 4 monolayers of Cu(001). Our calculation is based on *ab initio* eigenstates of the slab, which are obtained within the full-potential linearized augmented plane-wave method. The ground-state spin-polarized electronic structure is converged self-consistently to an accuracy better than 0.1 mRy. Subsequently, we take the spin-orbit interaction into account within a second variational treatment. The new set of eigenstates allows us to calculate the magneto-optical transition matrix elements. The second-harmonic response is determined in the reflection geometry with magnetization perpendicular to the surface (the so-called polar configuration) using the surface-sheet model. Adding layers of a noble metal (Cu) to the Fe monolayer gives a new degree of freedom for the inclusion of nonmagnetic Cu *d* bands to the nonlinear magneto-optical response of the slab, and the energy bands show that such an addition converges essentially to an addition of *d* states and a small broadening of the *d* band with growing number of Cu layers. The screened nonlinear optical susceptibility is calculated and converges quite well with a growing number of Cu layers. Our first-principles results confirm that the magnetic tensor elements of the nonlinear optical response tensor are roughly of the same order of magnitude as the nonmagnetic ones (in contrast to linear optics, where the magnetic response is only a minor correction).

DOI: 10.1103/PhysRevB.65.174409 PACS number(s): 78.20.Ls, 73.20.At, 78.66.Bz

I. INTRODUCTION

The nonlinear magneto-optical Kerr-effect (NOLIMOKE) has become a versatile tool for the investigation of thin film magnetism, as predicted[1,2] by theory. Nonlinear optics from magnetic surfaces and thin films has recently been studied experimentally by several groups,[3–16] and different theoretical and numerical aspects have been addressed as well.[15–24] As with nonmagnetic nonlinear second-order optics,[25–37] magnetic nonlinear optics is important for the characterization of (solid-state) structures containing surfaces, interfaces, and various subsurface structures. Within the electric-dipole approximation the second-harmonic signal from bulk inversion symmetric materials results from surfaces and interfaces.

The early theoretical treatments of nonlinear magneto-optics[1,2] have been extended by Pustogowa, Hübner, Bennemann, and Kraft[21] in order to establish an *ab initio* theory for optical second-harmonic generation (SHG) from magnetic thin films within the electric-dipole approximation. Their work included the electronic band structure via a full-potential linearized muffin-tin orbital (FP-LMTO) calculation, but was limited to constant optical transition matrix elements. The need for calculations of optical transition matrix elements based on *ab initio* treatment of the wave functions has recently been filled by the work of Dewitz, Chen, and Hübner,[38,39] using the full-potential linearized augmented plane-wave (FLAPW) method. Asada and Blügel[40] have been studying the magnetic states for fcc Fe films on Cu(100) using *ab initio* methods.

In Refs. 41–44, Petukhov and Liebsch study the nonlinear optical response of Al. Their work discusses the isotropic and anisotropic bulk contributions to SHG using a two-band model,[41] frequency dependence and penetration depth,[42] and in later works also the anisotropic nonlinear optical surface response within the two-band model[43] and a nearly-free-electron model.[44] The method is extended to include more than one interband transition in the work by Ishida, Petukhov, and Liebsch,[45] where an embedding approach is applied. They[45] estimate a SHG response depth of ''10 to 20 interplanar spacings'' (monolayers). Kuchler and Rebentrost[46–48] have developed models to describe SHG from adsorbates on surfaces of simple metals and semiconductors. For the metals, their model is based on the local density approximation (LDA) and the Lang-Williams chemisorption model.[49] These models may be fine for simple metals, but for transition metals a free-electron-like treatment does not suffice.

In recent years, the time-dependent local-density approximation (TDLDA) has been developed.[35,50–53] In a combination of this approach with a jellium model, Liebsch and co-workers have performed calculations of second-harmonic[54–57] and sum-frequency generation[58] from simple metal surfaces and obtained good agreement with measurements on Al and Ag, and of Na and K layers adsorbed on Al.[59]

In the present work we aim at describing second-harmonic generation from an Fe monolayer placed on top of semi-infinite Cu. Starting with an Fe/Cu(001) bilayer, we investigate the influence on the nonlinear optical response from each additional substrate Cu layer. The number of substrate layers we can address individually is, of course, limited. Experiments on the subject[7,11,60–66] show that (i) Fe grows pseudomorphically on Cu at room temperature—meaning that usage of the Cu lattice constant makes sense, and (ii) the natural magnetization direction under these circumstances is along the surface normal.

The electronic structure is calculated within the framework of the WIEN97 FLAPW method,[67] thus employing a supercell approach to the thin film system. The nonlinear optics is calculated in the electric-dipole (ED) approximation

using the so-called surface-sheet model, developed by Sipe, Moss, and van Driel.[68] Usage of the surface-sheet model and the ED is justified, since the major obstacle in the treatment of SHG from thin magnetic films in an *ab initio* framework is the inclusion and accuracy of the spin-orbit coupling in the wave functions of the electronic ground state. Furthermore, there is no way known to include a laser field into time-independent density-functional theory, thereby determining a natural penetration depth of the laser field, etc. The determination of the penetration depth is needed if one wants to abandon the use of a simple model surface response such as the surface-sheet model. On these grounds, the surface-sheet model has proved its value (see, e.g., Ref. 69 and references therein). In our paper it is assumed that the nonlinear optical response is generated alone by the physical region where the Fe layer is present (hereafter also referred to as the surface), and that the role of the Cu is twofold: (i) the Cu defines the lattice spacing since Fe grows pseudomorphically on fcc Cu(001), and (ii) the addition of Cu is expected to amplify the nonlinear optical response in comparison to the response from the Fe alone by contributing *d* electrons to the Fe layer. Hence, the addition of a noble metal provides us with a new degree of freedom.

The difficulty in handling calculations of NOLIMOKE on an *ab initio* basis lies in the fact that one needs highly accurate wave functions to reliably calculate the optical transition matrix elements occurring in any calculation of nonlinear optics.

Tight-binding methods are insufficient for the calculation of optical transition matrix elements, since (i) the potentials are inaccurate, leading to trouble with the spin-orbit coupling, (ii) they do not describe the hybridization of the *s* and *d* electrons well. In particular, they reproduce neither the correct symmetry nor the correct localization behavior of the wave functions and transition matrix elements of $3d$ electron systems with sufficient accuracy. (iii) Adjusted parameters are made to fit a level scheme. Finally, (iv) the transferability of the parameters to the system is not guaranteed, in particular the thickness dependence—they are based on results for the bulk.

In first-priciples thin film simulations like ours, quantum well states will inevitably be part of the picture.[70–72]

In Sec. II, we list the relevant formulas for our calculations. In Sec. III, we present numerical results of NOLIMOKE for an Fe monolayer placed on 1–4 monolayers of Cu(001). In Sec. III A we discuss the band structure of these thin films, including spin-orbit effects and convergence criteria to reach bulk Cu. In Sec. III B we show the spectral dependence of the nonzero tensor elements of the nonlinear optical susceptibility calculated on the basis of the presented band structure. In Sec. III C we discuss the ability to resolve symmetries and nonlinear optical reflection properties in the form of (frequency-dependent) intensities. Finally, in Sec. III D we show the nonlinear magneto-optical Kerr rotation angle. We finish our treatment by summarizing our findings and discussing possible extensions to our theoretical model in Sec. IV.

II. THEORETICAL BACKGROUND

Since *ab initio* nonlinear optics of transition metal systems is still in its infancy, we use the electric-dipole (ED) approximation. The use of the ED model seems appropriate, because (i) the purpose of this work is to check the effect and convergence behavior of adding Cu layers all the way starting from the band structure, via the optical tensor elements to the observable quantities, such as SHG intensities and the nonlinear Kerr effect, mainly focusing on their frequency dependence. Furthermore, (ii) the additional nonlocal contribution arising in jellium[73] for *s*-polarized light has neither been shown to be of relevance to transition metals, nor in combination with magnetism—not even in linear MOKE.

A. The nonlinear optical susceptibility

The present calculations of the nonlinear magneto-optical response are based on the expression for the nonlinear susceptibility derived in the usual perturbative manner (comprehensive details of the derivation can be found in the work of Hübner and Bennemann),[2] here taken in the long-wavelength limit[74–76] (consult also Ref. 77)

$$\chi^{(2)}_{ijk}(2\mathbf{q},2\omega)=e^3\sum_{\mathbf{k},l,l',l''}\left\{\frac{\langle\mathbf{k}+2\mathbf{q},l''|\mathbf{r}_i|\mathbf{k},l\rangle\langle\mathbf{k},l|\mathbf{r}_j|\mathbf{k}+\mathbf{q},l'\rangle\langle\mathbf{k}+\mathbf{q},l'|\mathbf{r}_k|\mathbf{k}+2\mathbf{q},l''\rangle}{E_{\mathbf{k}+2\mathbf{q},l''}-E_{\mathbf{k},l}-2\hbar\omega+2i\hbar\alpha}\right.$$
$$\left.\times\left(\frac{f(E_{\mathbf{k}+2\mathbf{q},l''})-f(E_{\mathbf{k}+\mathbf{q},l'})}{E_{\mathbf{k}+2\mathbf{q},l''}-E_{\mathbf{k}+\mathbf{q},l'}-\hbar\omega+i\hbar\alpha}-\frac{f(E_{\mathbf{k}+\mathbf{q},l'})-f(E_{\mathbf{k},l})}{E_{\mathbf{k}+\mathbf{q},l'}-E_{\mathbf{k},l}-\hbar\omega+i\hbar\alpha}\right)\right\}$$
$$\times\left[1+4\pi e^2\sum_{ab}m_am_b\sum_{\mathbf{k},l,l''}\langle\mathbf{k},l|\mathbf{r}_a|\mathbf{k}+2\mathbf{q},l''\rangle\langle\mathbf{k}+2\mathbf{q},l''|\mathbf{r}_b|\mathbf{k},l\rangle\frac{f(E_{\mathbf{k}+2\mathbf{q},l''})-f(E_{\mathbf{k},l})}{E_{\mathbf{k}+2\mathbf{q},l''}-E_{\mathbf{k},l}-2\hbar\omega+2i\hbar\alpha}\right]^{-1},\quad(1)$$

where $\mathbf{k}$ and $\mathbf{q}$ are the wave vectors of the electron and the photon, respectively, l is the angular momentum quantum number, m_a and m_b are direction cosines of $\mathbf{q}$ in the direction of a and b, respectively, where $a,b\in\{x,y,z\}$. Furthermore, $-e$ is the charge of the electron, $\hbar$ is Planck's constant $h/2\pi$, ω is the cyclic frequency of the photon, $\mathbf{r}$ is the position operator, and $E_{\mathbf{k},l}$ is the eigenenergy belonging to the quantum state $|\mathbf{k},l\rangle$. The spin index is dropped here, since

the spin-orbit coupling is included in the wave functions.

As opposed to previous numerical studies[21,24,38] we do not neglect the contribution in the square brackets here. It is the screening term that describes the linear interaction of the generated second-harmonic light. Our way to treat the spin-orbit coupling has been established in Ref. 38. It is treated within second variation, and only the isotropic contribution inside the muffin-tin sphere is included. This is justified because the spin-orbit coupling is largest close to the nucleus, where the potential is essentially spherical. The dipole transition matrix elements are calculated using the momentum operator **p** which is connected to the matrix elements of the position operator **r** via

$$\langle \psi_i|\mathbf{r}|\psi_j\rangle = \frac{i\hbar}{m_0}\frac{\langle \psi_i|\mathbf{p}|\psi_j\rangle}{E_j - E_i}. \tag{2}$$

The part of the momentum operator resulting from the spin-orbit contributions is neglected. Hence, no spin-flip processes are taken into account, which appears to be a good approximation.[78,79] The spin-orbit coupling enters through the ground-state solutions to a Schrödinger-like equation where spin-orbit interaction has been added explicitly. The magnetization enters through the spin quantization axis. Thus, the influence of the spin-orbit coupling and the magnetization is accounted for in the wave functions above.

In semiconductors,[77,80–82] the band structure essentially consists of valence and conduction bands, and thus in general formulas for the second-harmonic response are normally tailored to that specific (simplified) band structure. The conventionally applied indices v and c for the valence and conduction bands imply an energetic order of the bands that is not *a priori* known in metals. Thus, l, l', and l'' are included in a general manner, and the intraband contributions are included in Eq. (1) by allowing all combinations of l, l', and l'', including $l=l'$, etc.

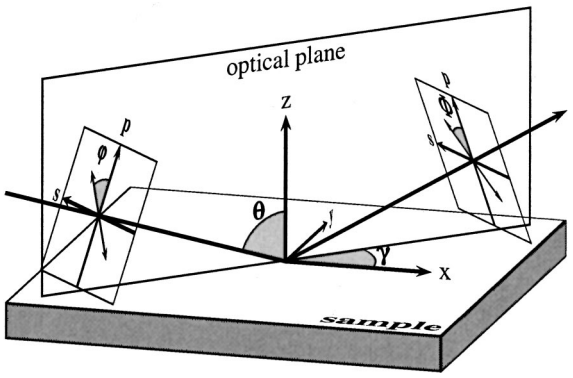

FIG. 1. The scattering geometry used in deriving Eq. (3). The polarizer angle of the incoming field is denoted by φ, the analyzer angle for the second-harmonic field by Φ, and the angle γ in the x-y plane describes the rotation of the optical plane with respect to the probe. The optical plane is defined as the plane spanned by the wave vectors of the incoming and reflected light, as usual.

B. The second-harmonic field

The second-harmonic field is calculated using the surface sheet model by Sipe, Moss, and van Driel.[68] The expression for the second-harmonic optical field established in Ref. 83 is here generalized (see also Ref. 75) to include an angle γ (azimuth) that describes the rotation of the optical plane with respect to the surface normal (see Fig. 1). The second-harmonic field projection onto the analyzer polarization angle Φ is

$$E(2\omega;\theta,\Phi,\varphi,\gamma) = 2i\delta z\frac{\omega}{c}|E_0(\omega)|^2\left\{A_s\sin\Phi\begin{pmatrix}-\sin\gamma\\ \cos\gamma\\ 0\end{pmatrix} + A_p\cos\Phi\begin{pmatrix}F_c\cos\gamma\\ F_c\sin\gamma\\ N^2F_s\end{pmatrix}\right\}$$
$$\cdot\underbrace{\left(\begin{array}{ccc|ccc} xxx & xyy & xzz & xyz & xxz & xxy\\ yxx & yyy & yzz & yyz & yxz & yxy\\ zxx & zyy & zzz & zyz & zxz & zxy\end{array}\right)}_{\chi^{(2)}}$$
$$\cdot\begin{pmatrix}[t_pf_c\cos\varphi\cos\gamma - t_s\sin\varphi\sin\gamma]^2\\ [t_pf_c\cos\varphi\sin\gamma + t_s\sin\varphi\cos\gamma]^2\\ t_p^2f_s^2\cos^2\varphi\\ 2[t_pf_c\cos\varphi\sin\gamma + t_s\sin\varphi\cos\gamma]t_pf_s\cos\varphi\\ 2[t_pf_c\cos\varphi\cos\gamma - t_s\sin\varphi\sin\gamma]t_pf_s\cos\varphi\\ 2[t_pf_c\cos\varphi\cos\gamma - t_s\sin\varphi\sin\gamma][t_pf_c\cos\varphi\sin\gamma + t_s\sin\varphi\cos\gamma]\end{pmatrix}, \tag{3}$$

in which we have used a standard contracted notation (|) above for $\chi^{(2)}$, $f_s=\sin\theta/n$ and $F_s=\sin\Theta/N$ are projections of the field at frequency ω and 2ω, respectively, as are $f_c=\sqrt{1-f_s^2}$ and $F_c=\sqrt{1-F_s^2}$. $t_p=2\cos\theta/(n\cos\theta+f_c)$ and $t_s=2\cos\theta/(\cos\theta+nf_c)$ are Fresnel transmission coefficients at frequency ω, $T_p=2\cos\Theta/(N\cos\Theta+F_c)$ and $T_s=2\cos\Theta/(\cos\Theta+NF_c)$ are transmission coefficients at 2ω, and $A_p=2\pi T_p/\cos\Theta$ and $A_s=2\pi T_s/\cos\Theta$ are transmission field amplitudes. Finally, $n=\sqrt{\varepsilon(\omega)}$ and $N=\sqrt{\varepsilon(2\omega)}$ are the frequency-dependent complex refractive indices of the substrate Cu at ω and 2ω. The different angles involved in the equations above (φ,γ,θ) are defined in Fig. 1. For the angle of reflection of the second-harmonic response, $\Theta=\theta$ holds due to the conservation of momentum along the surface, and in the rest of the paper we will use an angle of incidence of $\theta=\pi/4$, and an azimuth $\gamma=0$. The nonlinear optical intensity at the analyzer polarization angle, $I(2\omega)$, is then calculated as

$$I(2\omega;\theta,\Phi,\varphi,\gamma)=\epsilon_0 c_0|E(2\omega;\theta,\Phi,\varphi,\gamma)|^2. \tag{4}$$

In Eq. (3), $\chi^{(2)}$ is calculated in **k** space with the charge density profile taken fully into account, and the quantity δz is a normalization factor for the application of the surface-sheet model. It is in our calculations put equal to the bulk value of the thickness of a single Fe layer.

When calculating the nonlinear optical response of a surface within reciprocal space in a full-potential calculation where the unit cell is divided into muffin-tin spheres and an interstitial region (as in the FLAPW package WIEN97), one faces two problems. First, a system with a surface (such as a vacuum/film/substrate system) does not have translation invariance perpendicular to the film plane, which means that one has to use a supercell approach and ensure that enough space is added between two adjacent vacuum/film/substrate systems to avoid electronic overlap, i.e., the vacuum has to be of a certain thickness. In our work we use the equivalent of 8 Cu monolayers as the extent of the vacuum, which should be enough in order to ensure electronic decoupling between films in the supercell. Second, since SHG takes place in the surface of a structure, the interstitial region has to be treated with care. In the work of Dewitz,[75] an approximation has been established for the purpose of calculating the second-harmonic response from a surface. The division of the unit cell is shown in Fig. 2, and in the present work the nonlinear response is included only from the muffin-tin spheres of the Fe layer and from the half-space of the interstitial region that comprises the vacuum and the vacuum/film interface. After restricting the integration of the dipole transition matrix elements the wave functions are orthogonalized by applying

$$\langle\psi_f|\mathbf{p}|\psi_i\rangle\rightarrow\langle\psi_f|\mathbf{p}|\psi_i\rangle-\frac{\langle\psi_f|\psi_i\rangle}{\langle\psi_i|\psi_i\rangle}\langle\psi_f|\mathbf{p}|\psi_i\rangle. \tag{5}$$

In our electrodynamical treatment we make the following distinction between the surface sheet and the substrate: The Fe monolayer and the spillout of the wave functions into the vacuum layers comprise the surface sheet, and the second-harmonic generation is assumed to take place solely because of this and the contributions from the underlying Cu layers to the Fe bands. The substrate in the surface-sheet model is taken to be semi-infinite bulk Cu.

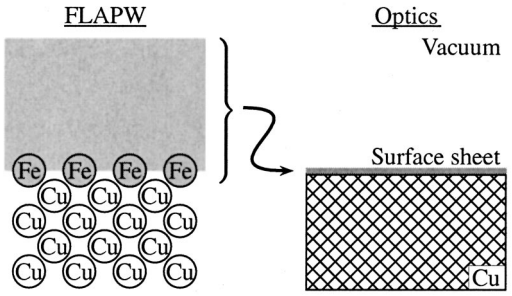

FIG. 2. The supercell structure used in the calculation of the electronic structure is shown to the left for 1 monolayer (ML) Fe on 4 ML Cu(001). In all cases, the vacuum in the supercell consists of the equivalent of 8 ML in a bulk Cu crystal. The right panel shows the surface-sheet model implementation we use. The shaded area in the left panel, consisting of the vacuum layers and the Fe monolayer, is in our optics calculations contracted to the surface sheet shown on the right.

C. The nonlinear Kerr effect

The Kerr angles are calculated from standard complex-plane Poincaré ellipsometry.[84–86] The Kerr rotation ϕ_K and the ellipticity ϵ_K are calculated from the ratio κ of the complex E_s and E_p components of the second-harmonic field, $\kappa\equiv E_s/E_p$, as

$$\tan(2\phi_K)=\frac{2\ \mathrm{Re}(\kappa)}{1-|\kappa|^2}, \tag{6}$$

$$\sin(2\epsilon_K)=\frac{2\ \mathrm{Im}(\kappa)}{1+|\kappa|^2}. \tag{7}$$

Thus, the nonlinear Kerr rotation can be determined as

$$\phi^{(2)}=\frac{1}{2}\arctan\frac{2\ \mathrm{Re}(\kappa)}{1-|\kappa|^2}+\phi_0, \tag{8}$$

where $\phi_0=0$ for $|\kappa|^2\leqslant 1$, $\phi_0=\pi/2$ for $|\kappa|^2>1$ and $\mathrm{Re}(\kappa)\geqslant 0$, and $\phi_0=-\pi/2$ for $|\kappa|^2>1$ and $\mathrm{Re}(\kappa)<0$.

III. NUMERICAL RESULTS AND DISCUSSION

Below, the numerical calculations are restricted to the case where the magnetization direction of the Fe layer is perpendicular to the surface ($\mathbf{M}\|z$, the so-called polar magneto-optical configuration), in accordance with experiment[87] for Fe on Cu at room temperature. For the (001) orientation considered, the number of independent elements of the nonlinear susceptibility tensor is reduced to 4 due to the symmetry, and $\chi^{(2)}$ can then be written[76]

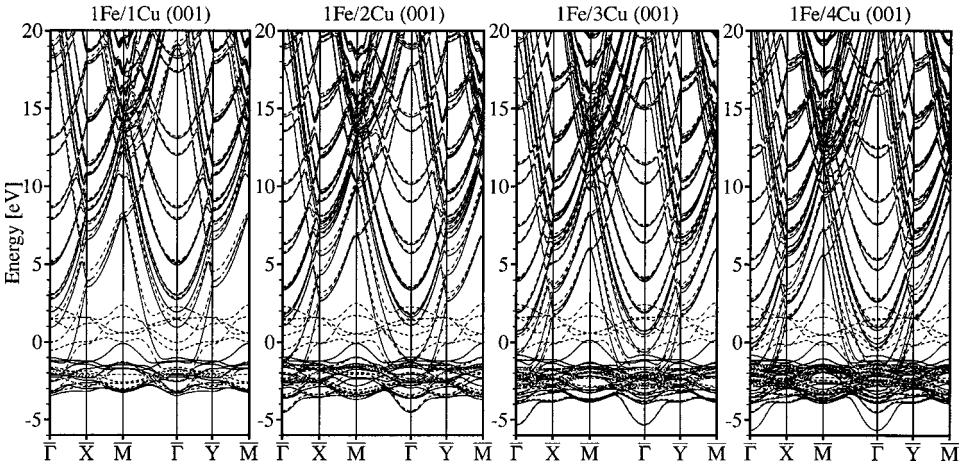

FIG. 3. The band structure of a monolayer (ML) of Fe on top of (left to right) 1 ML, 2 ML, 3 ML, and 4 ML of Cu(001). In all plots, the abscissa is the path through the (two-dimensional) Brillouin zone, and on the ordinate are the eigenenergies in eV at each point on the abscissa. The solid lines represent eigenenergies where the corresponding two-component wave function contains more than 90% majority spin, dashed lines states with more than 90% minority spin, and dotted lines anything in between. The Cu *d* band lies approximately in the range of 4 eV to 1.7 eV below the Fermi energy, which in all cases is at zero on the ordinate.

$$\chi^{(2)}=\left(\begin{array}{ccc|ccc} 0 & 0 & 0 & xyz^- & xxz^+ & 0 \\ 0 & 0 & 0 & xxz^+ & -xyz^- & 0 \\ zxx^+ & zxx^+ & zzz^+ & 0 & 0 & 0 \end{array}\right), \tag{9}$$

where the superscripts + and − denote even and odd tensor elements, respectively.

Since we are aiming at describing the influence of a bulk fcc Cu substrate on the nonlinear optical response of an Fe(001) monolayer, all slab calculations are done with fcc Cu lattice positions in the (001) orientation, and consequently also using the bulk Cu lattice constant of 3.61 Å.

To calculate the electronic structure we use the numerical package WIEN97, by Blaha, Schwarz, and Luitz.[67] It is a full-potential LAPW code,[88] and in order to put our calculations on solid ground we perform a self-consistent convergence of the total energy to within 0.1 mRy. This is done using the generalized gradient approximation exchange and correlation potential of Perdew, Burke, and Ernzerhof[89] (GGA-PBE), with a muffin-tin sphere of radius 1.21 Å, a kinetic energy cutoff of 81 Ry, and a plane-wave cutoff at 13 Ry. The maximal l quantum number is 6 for 1–3 Cu layers, and 10 for 4 Cu layers. The eigenvalues are calculated in a range from −7 Ry to +1.5 Ry relative to the Fermi energy, and the optical response is calculated within ±1.5 Ry, which ensures a decent accuracy for optical responses with a fundamental input energy of up to 10 eV. The number of **k** points needed for a converged optical response has been determined in the way that a sufficient number of **k** points is reached when a 10% change in the number does not influence the graphs of the optical response. Final calculations, including treatment of the spin-orbit coupling, are thus done with 2502 **k** points in the irreducible wedge of the Brillouin zone, using the tetrahedron method of Blöchl, Jepsen, and Andersen,[90] and without introducing inversion symmetry perpendicular to the film plane.

Tests show there is still a non-negligible residual influence in the amplitude of the nonlinear optical response when one varies the boundary between the two basis sets given by the radius of the muffin-tin sphere. This is a result of using (i) two different basis set expansions that are not mutually orthogonal, (ii) different approximations when using the different basis sets, and (iii) the second-variational treatment[91,92] of the spin-orbit coupling. Choosing too small a basis set, the wave functions may not be described accurately enough, whereas choosing too large a basis set may worsen the effects of the inorthogonality between the two basis sets. This problem of course gets amplified when three transition matrix elements are multiplied to get the result, as is the case in this paper. We will not elaborate further on these issues here, and in the remaining part of the paper simply work with the muffin-tin radius mentioned above (1.21 Å).

A. Convergence of the band structure

The band structure for 1 ML Fe on top of 1–4 ML of Cu is shown in Fig. 3 along the path in the (two-dimensional) Brillouin zone, starting from the Γ point, going to X and M (which is the fourth corner of the rectangle in the two-dimensional (2D) Brillouin zone spanned by Γ-X and Γ-Y), back to the Γ point, out to Y, and ending at M. In the polar (001) configuration, Y should be equal to X. In this figure, the majority spin states (more than 90% majority spin) are plotted using dashed lines, and the minority spin states (more than 90% minority spin) are depicted using solid lines. The dotted lines represent states with less than 90% of either spin, and are mainly present in the densely populated Fe *d* band between 1 and 3 eV below the Fermi energy, as one might expect. Looking at the M point, we observe a group of states between 0.5 eV below and 2.5 eV above the Fermi level. These are Fe *d* states of the minority spin (mostly unoccupied), and they do not change much when adding Cu layers. Their presence reflects the magnetic moment of the structure, and the slight disturbance in these bands can be attributed to the transfer of magnetic moment to the Cu sub-

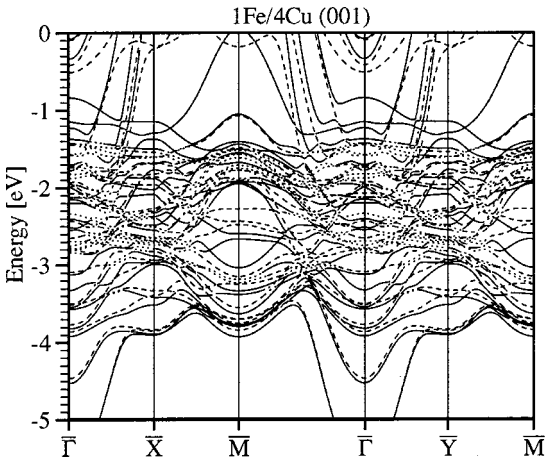

FIG. 4. The *d* band region below the Fermi energy of a monolayer (ML) of Fe on top of 4 ML of Cu(001). The abscissa is the path through the Brillouin zone, and the ordinate the eigenenergies in eV at each point on the abscissa. The solid lines represents eigenenergies of more than 90% majority spin, dashed lines states with more than 90% minority spin, and dotted lines anything in between. As before, the ordinate is relative to the Fermi energy.

strate layers. In contrast, the occupied Fe majority *d* states mix with the Cu *d* states. The exchange splitting of the Fe *d* band is in all four cases just about 2.5 eV. We notice that the added Cu layers contribute with a *d* band whose onset is at around 1.7 eV. Comparing with photoemission experiments,[93–96] one would have expected this to be at 2.17 eV. However, this is a well-known[97,98] error of the local spin density approximation (and GGA) in density-functional theory, and its main effect on the second-harmonic response is a redshift of the peaks in the spectrum. This redshift is independent of the redshift we expect when adding more Cu layers.

For better visibility of the mixed-spin states, in Fig. 4 we show the region from 0 to 5 eV below the Fermi energy in the case of Fe on top of 4 Cu layers, which has the highest content of mixed spin states. It appears from Fig. 4 that these mixed spin states are mainly in the Cu *d* band region, and that the spin polarization of each band varies in **k** space, such that bands whose states are well-defined as either majority or minority spin states at M become mixed when going away from M.

Looking at the lower end of the energy scale in Fig. 3, we find the *s* states, which in the case of 4 Cu layers look like they do in bulk. However, when going to less Cu layers, we observe that these states are shifted to higher energies around the $\bar{\Gamma}$ point, and in the bilayer they are hardly distinguishable from the Cu *d* states.

We may conclude from Fig. 3 that adding Cu layers gives many more occupied *d* states and highly dispersive unoccupied free-electron states. Additionally, the distance between energy bands is decreased with increasing number of Cu layers, giving many more possible transitions in the nonlinear optical response. With the addition of the 5th Cu layer, the energy bands become diffuse in the numerical step where we include spin-orbit coupling, and thus, magneto-optical results from our code beyond 4 Cu layers become inconclusive. The energy difference between eigenstates at X and Y in Fig. 3 has been checked explicitly in order to verify that they are identically zero, as they should be due to our chosen direction of magnetization ($\mathbf{M} \| z$).

In the optical response, the observed broadening of the Cu *d* band with addition of Cu layers should result in a monotonous redshift (a shift to lower energies) of the peak in the spectrum expected at an input energy of 2 eV as more Cu layers are added. For a convergent result, the increment in this shift should be smaller and smaller for each new Cu layer.

Here, Cu is nearly nonmagnetic, and does not contribute directly to the SHG response in our use of the surface-sheet model. However, due to the spillout of electrons from the Cu to the Fe, fingerprints of the Cu will be seen even in the nonlinear *magneto*-optical spectrum because of variations in the wave functions that are included in the surface sheet. In order to test this expectation in the various quantities relevant to NOLIMOKE we perform calculations of magnetic moments, the screened nonlinear optical tensor elements, and nonlinear optical intensities.

Magnetic spin moments (in Bohr magnetons, μ_B) of the different layers are listed in Table I. It shows that the overwhelming part of the total magnetic moment is carried by the Fe layer, as one should expect. It also shows that the magnetic moment is smaller than for a free-standing Fe layer ($3.2\mu_B$). Furthermore, (i) the first Cu substrate layer is always ferromagnetically coupled to the Fe layer—in agreement with the results of Asada and Blügel,[40] and (ii) the

TABLE I. Magnetic spin moments (in Bohr magnetons) for each layer in the Fe/Cu(001) unit cell. Results are shown for one Fe layer on top of up to 7 Cu layers.

	Cu layer number						
Fe	1	2	3	4	5	6	7
2.828	0.046						
2.844	0.043	−0.026					
2.793	0.033	−0.025	−0.003				
2.792	0.048	−0.015	−0.006	−0.065			
2.853	0.042	−0.016	−0.000	0.001	0.001		
2.835	0.044	−0.016	−0.002	−0.001	−0.002	−0.006	
2.740	0.045	−0.016	0.004	0.005	0.008	0.001	−0.010

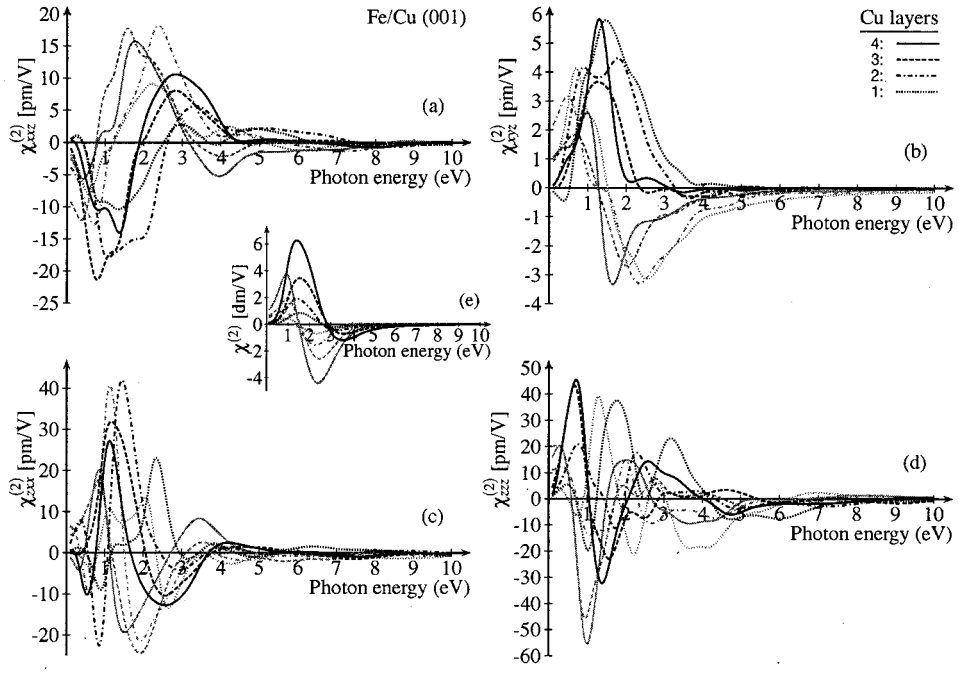

FIG. 5. Nonzero tensor elements ($\chi^{(2)}_{ijk}$) of the screened nonlinear susceptibility tensor [Eq. (1)] as a function of incident photon energy for 1 ML Fe on 1–4 ML Cu in the limit where $|\mathbf{q}|=0$. (a) $\chi^{(2)}_{xxz}$, (b) $\chi^{(2)}_{xyz}$, (c) $\chi^{(2)}_{zxx}$, and (d) $\chi^{(2)}_{zzz}$. The small inset (e) shows $\chi^{(2)}$ with constant transition matrix elements. Throughout the figure, real parts are in gray and imaginary parts are in black. The line styles are encoded according to the number of Cu layers, the solid line representing 4 ML Cu, the dashed line 3 ML Cu, the dash-dotted line 2 ML Cu, and the dotted line 1 ML Cu.

second Cu layer is always antiferromagnetically coupled to the Fe layer. Looking at data only up to four Cu layers, there is a tendency of convergence in the sense that adding Cu layers 3 and 4 gives further contributions to the antiferromagnetic coupling. This tendency disappears again from the fifth Cu layer, and looking at the full data set, an oscillation in the magnetic moment of the Fe layer is present. Such a behavior could be reponsible for the oscillatory variations of the nonlinear magneto-optical response observed in experiments[99] as a function of the thickness of the noble metal.

In comparison, calculations on (i) 1 ML Fe on bcc Mo(110) gives[100] a magnetic moment of the Fe layer of $2.593\mu_B$, and the first three layers of Mo are antiferromagnetically coupled to the Fe layer, and on (ii) 1 ML Fe on bcc W(110) gives[101] a magnetic moment of the Fe layer of $2.536\mu_B$, and as before, the first three layers of W are antiferromagnetically coupled to the Fe layer. The difference with our case of fcc Fe(001) is thus that (i) we have a higher magnetic moment of the Fe layer, and (ii) the first substrate layer is ferromagnetically coupled to the Fe. However, the next three layers are antiferromagnetically coupled, as in these two cases, at least until more layers are added.

B. The nonlinear susceptibility tensor

The real and imaginary parts of the four independent nonzero tensor elements ($\chi^{(2)}_{ijk}$) of the screened nonlinear susceptibility tensor are shown as a function of the incident photon energy in Figs. 5(a)–5(d) in the limit where $|\mathbf{q}|\rightarrow 0$. The small inset [Fig. 5(e)] shows the response for constant matrix elements.

First of all, let us emphasize that the very presence of $\chi^{(2)}_{xyz}$ in Fig. 5 clearly demonstrates that nonlinear optical susceptibility tensors are now accessible using *ab initio* methods — including magnetism and substrate effects. The result for constant matrix elements [Fig. 5(e)] is that the peak position of both the real and imaginary part of the susceptibility oscillates, shifting to lower energies for even numbers of Cu monolayers (2 and 4), and higher energies for odd numbers (1 and 3) of Cu monolayers.

Looking at Fig. 5, we observe in general for all tensor elements that the most spectacular features are at fundamental input photon energies below 5 eV, and that the strength of the tensor elements fades out at higher photon energies. This general tendency is in good agreement with the energy bands from Fig. 3. In agreement with previous results[39] for Fe monolayers we see that the magnetic tensor element ($\chi^{(2)}_{xyz}$) is approximately of the same order of magnitude as the nonmagnetic tensor elements. This again confirms the higher magnetic contrast in NOLIMOKE in comparison with linear MOKE. The largest peaks appear in all cases in the region of incident photon energy starting at around 0.7 eV and ending at around 1.6 eV, fitting quite well with the transitions from the occupied Fe/Cu *d* band to the unoccupied portion of the Fe *d* band.

Going more into detail, one should bear in mind that the nonlinear optical tensor elements consist of sums over many states that in general cannot individually be identified. We observe from Fig. 5 the following: (i) The magnetic tensor element $\chi^{(2)}_{xyz}$ shows in the real part a pronounced peak around 1 eV that moves a little bit down for the second Cu layer, but appears to be moving back up again for the third and fourth layer. The slope at the zero crossing on the high-energy side of this peak, however, obeys the general tendency of a monotonous redshift for increasing thickness of the Cu that we expect from the broadening of the Cu *d* band. A smaller peak is observed starting around 3 eV and moving to lower energies to about 2 eV for four Cu layers. In the imaginary part, a peak starts at a little above 2 eV for the bilayer, and it moves gradually downwards in energy until it has reached 1.5 eV for the fourth Cu layer. (ii) The usually

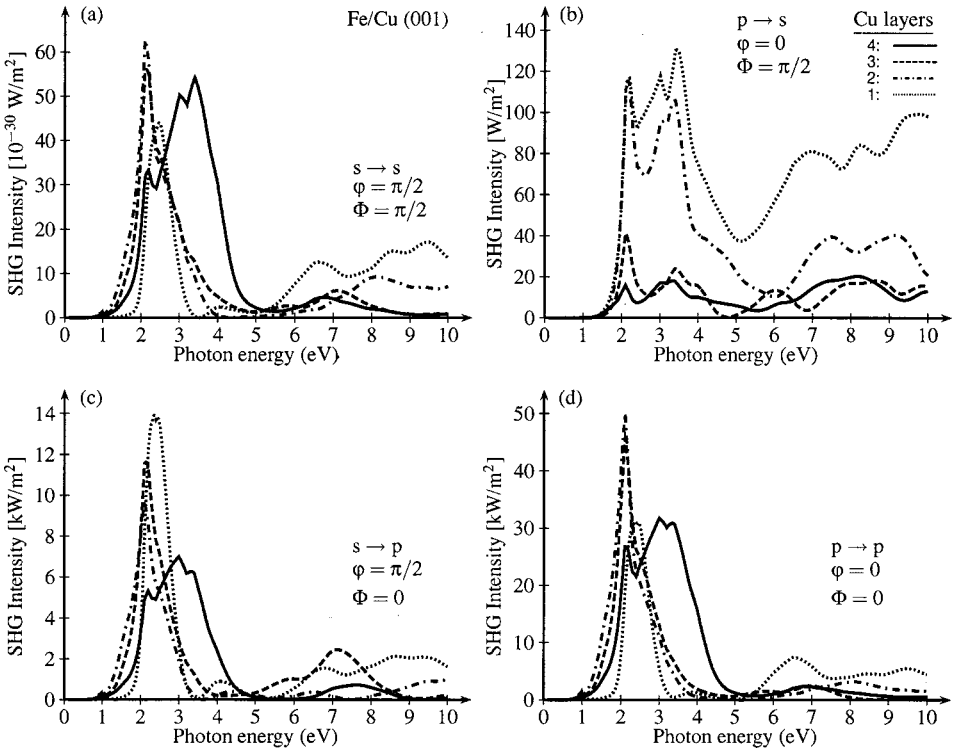

FIG. 6. Nonlinear optical response of a single Fe monolayer on top of 1–4 Cu monolayers is plotted as a function of the incident photon energy for (a) *s* polarized input as well as output, (b) *p* polarized input with *s* polarized output, (c) *s* polarized input with *p* polarized output, and (d) *p* polarized input and output. In all plots, $\gamma=0$ and $\theta=\pi/4$. As in Fig. 5, the line styles are encoded according to the number of Cu layers, the solid line representing 4 ML Cu, the dashed line 3 ML Cu, the dash-dotted line 2 ML Cu, and the dotted line 1 ML Cu.

dominating tensor element $\chi^{(2)}_{zzz}$ is in our calculation the largest as well, but not in any way so large that it can be said to be ''dominating.'' It has a strong peak in the real part also around 1 eV, but it tends to be a little bit displaced to higher energies compared to the peak for the magnetic tensor element. The imaginary part shows a strong peak at just below 1 eV, except for the Fe/Cu(001) bilayer, where pronounced peaks are found at around 2 and 3.5 eV. That the response does not peak at the exact same frequencies as for the magnetic tensor element is very pleasing, since the peaks of the *zzz* element are almost an order of magnitude larger than those of the *xyz* element. (iii) The nonmagnetic tensor element $\chi^{(2)}_{xxz}$ has strong peaks in its real part around 1 and 2 eV, while the imaginary part has them around 1.5 and 3.5 eV. (iv) For the last tensor element, $\chi^{(2)}_{zxx}$, the real part shows a peak located slightly above 1 eV that shifts down a little when adding Cu layers. Another peak between 2 and 3 eV shows the same behavior. In the imaginary part, the largest peak starts above 2 eV and shifts downwards to around 1.5 eV at the presense of the fourth Cu layer. It is surrounded by two other peaks that get stronger when Cu layers are added, while the main peak gets weaker.

Experiments[99,102] suggest that the influence of the thickness of Cu on SHG persists until at least 20–30 ML, and that the (linear[103,104] as well as SHG[7,105]) response oscillates with variation of the noble metal thickness. Thus, convergence is not expected at 4 ML, although our calculations show that results for 3 and 4 ML are pretty close to each other—in particular the results for the *zzz* element, which in free-electron-like metals usually dominates.[106]

It is remarkable that the effect of the nonmagnetic Cu shows up in the nonlinear *magneto*-optical response. Cu is known[76] to give a response that is a factor of 50 smaller than that of Fe, i.e., adding Cu layers to the Fe, one would naïvely expect the response of Fe with minor corrections, but even the presense of a few Cu layers changes the response much more. This quite strong effect of the presence of the Cu *d* band edge has been observed also in linear magneto-optics,[107] but is even stronger in the nonlinear case.

C. Nonlinear optical spectra

Nonlinear optical intensities are obtained by Eq. (4), where E is to be taken from Eq. (3). In Eq. (3) we use an input electric field E_0 of 10^8 V/m, and the frequency-dependent complex refractive indices (n and N) of the Cu substrate in the surface-sheet model are taken from the experimental data in Ref. 108, since no reliable computation based on DFT is available (*d* band position, see above). Therefore, the $\chi^{(2)}$ computed previously gives rise to the nonlinear polarization of the surface sheet—including the contributions from substrate layers via hybridization of the bands, while the medium underneath is treated in the framework of the above-mentioned experimental data. Thus, for the linear propagation of the second-harmonic field, the Cu block underneath gives rise to a bulk substrate effect in addition to the first-principles contributions from the Cu layers placed under the Fe (substrate surface effects). Consequently, interference from (several) complex tensor elements with the linear optical properties occurs, and we do not expect a one-to-one correspondence between the peaks observed in the nonlinear optical susceptibility and the peaks that will be present in the nonlinear optical spectra.

In Fig. 6 are plotted the resulting nonlinear optical intensities for *s* and *p* input and output polarizations. The main peak rising position from the low-energy side of the spec-

trum (long wavelength) fits very well with the experimental data on pure Cu(001) of Petrocelli, Martellucci, and Francini.[109] That this is the case clearly demonstrate the strong influence of the *linear* optical properties in the surface-sheet model, since if our nonlinear optical susceptibility were dominating, then the main peak position would have undergone a redshift due to the wrong position of the Cu *d* band. Furthermore, it is interesting to notice (as opposed to the naïve expectation of seeing a slightly modified Fe response) that the second-harmonic response fits to Cu data.

By plotting the symmetry-forbidden *s* polarized response from *s* polarized input [panel (a) in Fig. 6], we get an estimate of the noise level in our calculation. We observe that our calculations separate this forbidden response from the allowed responses by 30 orders of magnitude. Otherwise, as expected from the nonlinear susceptibility, the main features in the nonlinear optical spectra occur below a photon energy of 5 eV, and the largest response arises for *p* polarized input and output. Convergence as a function of the number of Cu underlayers is worse than that for the screened nonlinear optical susceptibility tensor, since the intensities (i) are functions of squares of many complex $\chi^{(2)}$, and (ii) additional linear optical effects are present via the Fresnel coefficients.

Two configurations have the presence of only one nonlinear optical tensor element, namely (i) the case of *s* polarized input and *p* polarized output, where only $\chi^{(2)}_{zxx}=\chi^{(2)}_{zyy}$ contributes, and (ii) when *p* polarized input gives *s* polarized output — here, only $\chi^{(2)}_{yxz}=-\chi^{(2)}_{xyz}$ contributes. Comparing the respective panels of Figs. 5 and 6, we observe that just as the peaks in Fig. 5(c) tend to be sharper than the peaks in Fig. 5(b), and Fig. 6(c) has a narrower main peak than Fig. 6(b). Looking at the amplitude, we notice that the order-of-magnitude difference between the largest features in $\chi^{(2)}_{zxx}$ and $\chi^{(2)}_{yxz}$ are reproduced in the peak heights of the intensities as the square of this, as one would expect.

Varying the azimuth γ simply reproduces the fact that the sample is completely isotropic when $\mathbf{M}\|\mathbf{z}$ (not shown). Varying the angle of incidence θ produces a trivial result depending only on the geometry, since in our calculations of $\chi^{(2)}$, $|\mathbf{q}|\rightarrow 0$.

In Fig. 7, the input polarization angle is varied for fixed output polarizations *p* and *s*, fixed incidence angle $\theta=\pi/4$ and photon energy 1.5 eV. The SHG signal reproduces the twofold symmetry, as expected. Taking a closer look at the lower panel of Fig. 7 (*s* polarized output), we recognize two zeros at $\varphi=\pi/2$ and $\varphi=3\pi/2$, which correspond to the *s* polarized input. While these two zeros stay at the same angle for all Cu layers, two other minima appear to be moving when the number of Cu layers change. In addition, the maxima also move as a function of the number of Cu layers. That there are two minima and two zeros instead of four equivalent zeros at half-integer multiples of π shows the breaking of symmetry by the presence of magnetism, since for *p* polarized input and *s* polarized output, only the magnetic tensor element $\chi^{(2)}_{xyz}$ contributes to the nonlinear optical response. In the case of *p* polarized output [upper panel (a) of Fig. 7] we also observe minima for *s* polarized input beams.

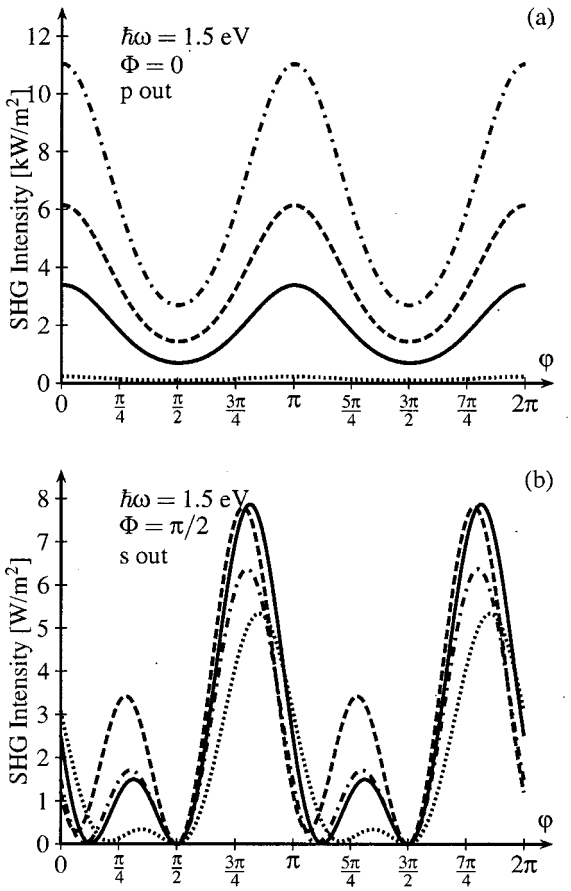

FIG. 7. Variation of the input polarization angle, φ, for an input photon energy of 1.5 eV, an input angle $\theta=\pi/4$, and analyzer polarizations (a) *p* and (b) *s* . As in Fig. 5, the line styles are encoded according to the number of Cu layers, the solid line representing 4 ML Cu, the dashed line 3 ML Cu, the dash-dotted line 2 ML Cu, and the dotted line 1 ML Cu.

These are the only minima, and they are true minima, not zeros, since at $\varphi=\pi/2$ a nonzero $\chi^{(2)}_{zxx}$ ensures a nonzero result, even for Cu alone. Maxima occur for all numbers of Cu layers at integer multiples of π. Thus, with the analyzer oriented in the *s* direction one has a better tool to reveal the presence of magnetism than if it is transmitting the *p* polarization. Furthermore, we observe from Fig. 7(a) that the intensity (i) is small for the Fe/Cu(001) bilayer, (ii) becomes sharply higher when the second Cu layer is added, and (iii) thereafter drops monotonically. This is in contrast to the case of *s* polarized output [Fig. 7(b)], where the intensity in many regions of the polarizer angle increases for each new Cu layer added. The form of the curves agrees with experiments on polycrystalline Cu (Ref. 110) as well as on Cu(001).[63]

That the minima in Fig. 7(a) do not go to zero in our electric-dipole model is attributed to transitions involving *d* states, which are enhanced due to the presense of the Fe layer (dipole transitions involving *s* states are forbidden).[83] Additionally, the presence of the Fe layer is responsible (in particular, the majority *d* state that approaches the Fermi energy at the M point in Fig. 3) for the fact that going to energies that exclude the Cu *d* band, the response (in plots equivalent to Fig. 7) *does not* reproduce the $\cos^4\varphi$-like behavior of go-

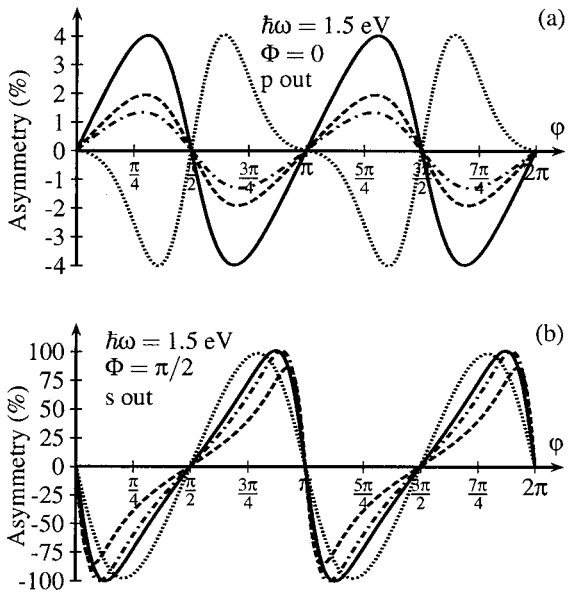

FIG. 8. Magneto-optical asymmetry $\mathcal{A}$ for variation of the input polarization angle, φ, for an input photon energy of 1.5 eV, an input angle $\theta=\pi/4$, and output polarizations (a) *p* and (b) *s*. As in Fig. 5, the line styles are encoded according to the number of Cu layers, the solid line representing 4 ML Cu, the dashed line 3 ML Cu, the dash-dotted line 2 ML Cu, and the dotted line 1 ML Cu.

ing to zero for *s*-polarized incident light that is present in the numerical work of Ref. 83 for the Cu(001) surface, as well as in the experiment of Ref. 109 for an oxidized Cu surface.

Experimental work by Vollmer, Straub, and Kirschner[63] for a clean Cu(001) surface suggests that intensities for *s* and *p* polarized output, when scanning φ, have the same order of magnitude. While we in Fig. 7 find much higher maxima for *p* polarized than for *s* polarized SHG output intensity, a conjecture suggests that the difference in intensities will get smaller when one adds Cu layers, thus giving a strong contribution from the substrate (limited to the penetration depth, or course). In addition to the contribution we can predict from our model, electric-quadrupole contributions are expected to give significant, possibly anisotropic, contributions to the bulk part of the response.[99] For the Fe layer, the bulk does not contribute to anisotropies, so our model with one Fe layer on a number of Cu layers should fix the Fe contributions while it adds information about the contributions from underlayers of Cu, and Cu changes the Fe intensity dramatically.

To emphasize the influence of magnetism on the second-harmonic response we have in Fig. 8 shown the magneto-optical asymmetry

$$\mathcal{A}=\frac{I(\mathbf{M}\|\mathbf{z})-I(\mathbf{M}\|-\mathbf{z})}{I(\mathbf{M}\|\mathbf{z})+I(\mathbf{M}\|-\mathbf{z})}, \tag{10}$$

for varying the input polarization angle φ. For comparative simplicity, we have plotted them on the same scale $[0{:}2\pi]$ as in Fig. 7. It should be noticed that at the four configurations given in the intensity plots of Fig. 6, the asymmetry is exactly zero (due to the adopted perpendicular direction of the magnetization). For the *p* polarized analyzer angle, we notice

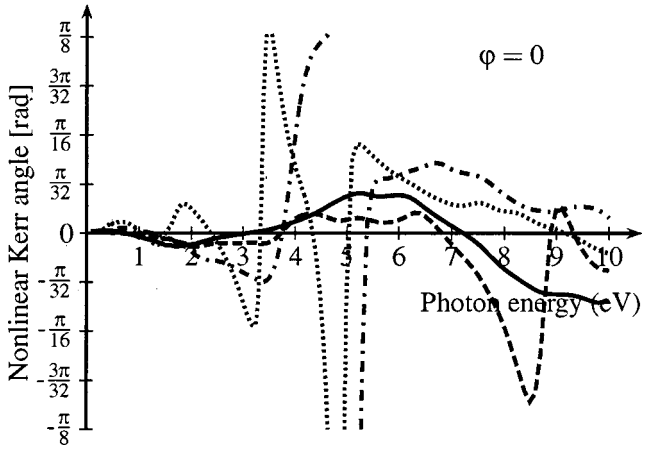

FIG. 9. The nonlinear magneto-optical Kerr rotation for 1 ML Fe on 1–4 ML Cu. As in Fig. 5, the line styles are encoded according to the number of Cu layers, the solid line representing 4 ML Cu, the dashed line 3 ML Cu, the dash-dotted line 2 ML Cu, and the dotted line 1 ML Cu.

that the asymmetry is very small (a few percent), whereas the asymmetry for the *s* polarized analyzer angle becomes close to unity at the minima occurring in Fig. 7(b). The effect of changing the magnetization direction is in this case very dramatic. However, in order to observe the influence of changing the magnetization direction the input polarizer must be turned away from the pure *s* and *p* directions. With respect to the curves of Fig. 7, reversing the magnetization direction is equivalent to a mirror operation in the curves of Fig. 7 around the value $\varphi=\pi/2$.

D. Nonlinear magneto-optical Kerr effect

Lastly, we proceed to present the most fragile results, namely the nonlinear magneto-optical Kerr rotation. Seen in the light of Figs. 6 and 7, one should expect the Kerr rotation to vary quite wildly with the input photon energy as well as the number of Cu layers. The result is presented in Fig. 9. The nonlinear Kerr rotation shown in Fig. 9 has been limited to the range $[-\pi/8{:}+\pi/8]$ in order to show the variation better. For 1 ML Cu, the peak at 4.8 eV goes down to approximately $-\pi/4$. For 2 ML of Cu, the peak at 5 eV goes all the way (2π) around. Also, there are some regions on the energy scale where the results for 3 and 4 ML of Cu are quite close. This could be a sign of convergence for thicker Cu layers.

IV. SUMMARY AND FUTURE PERSPECTIVES

We have presented an attempt at an *ab initio* nonlinear optics calculation for a monolayer of Fe placed on a Cu(001) substrate. We have demonstrated that a calculation of the nonlinear susceptibility is feasible, even when magnetism is included. The energy bands show a nice convergence to a simple addition of Cu *d* states and a slight broadening of the *d* band takes place when one adds more Cu layers. The nonlinear optical susceptibilities show the expected behavior of a redshift in many of the features, but not all, and the ten-

dency to convergence at the fourth Cu layer is not as pronounced as in the energy bands. The intensities, however, do not show similar signs of convergence, which we attribute to (i) the dependence on the square of a sum of many complex tensor elements, (ii) the continuing buildup of uncertainties in each of the nonlinear susceptibilities—more layers, more terms in the sum of each tensor element, (iii) the presence of linear optical artifacts in the denominators of the field projections and Fresnel coefficients, and (iv) the existence of quantum well states in the nonmagnetic substrate. This, of course, also affects the nonlinear magneto-optical Kerr rotation.

Even though this is an *ab initio* calculation, there are some points that attract attention as to what can be improved in the future. Among points in the model that need attention in order to give a more realistic description are (i) the position of the Cu *d* band and the excited states, (ii) the supercell concept (the periodicity along the surface normal should be abandoned), (iii) the non-spherical contributions to the spin-orbit interaction. When these points have been explored it will also make sense to take a closer look at (iv) the electric-dipole approximation, and (v) the surface-sheet model. These are all very tough problems to deal with in *ab initio* calculations.

ACKNOWLEDGMENTS

Stimulating discussions with M. Nyvlt and R. Vollmer are gratefully acknowledged. Additionally, we acknowledge computational vector optimization support by Rechenzentrum Garching, Garching (Munich), Germany, and financial support by the European Union ''Training and Mobility of Researchers'' network programs ''Nonlinear Magneto Optical Kerr Effect (NOMOKE)'' and ''High Frequency Dynamics of Mesoscopic Systems (DYNASPIN)'' under Contract Nos. ERB-FMRX-CT96-0015 and ERB-FMRX-CT97-0124, respectively.

*Electronic address: thor@mpi-halle.mpg.de
†Electronic address: huebner@mpi-halle.mpg.de

[1] R.-P. Pan, H.D. Wei, and Y.R. Shen, Phys. Rev. B **39**, 1229 (1989).
[2] W. Hübner and K.H. Bennemann, Phys. Rev. B **40**, 5973 (1989).
[3] V.V. Pavlov, G. Tessier, C. Malouin, P. Georges, A. Brun, D. Renard, P. Meyer, J. Ferre, and P. Beauvillain, Appl. Phys. Lett. **75**, 190 (1999).
[4] A. Kirilyuk, V. Kirilyuk, and T. Rasing, J. Magn. Magn. Mater. **199**, 620 (1999).
[5] N.N. Dadoenkova, I.L. Lyubchanskii, M.I. Lyubchanskii, and T. Rasing, Appl. Phys. Lett. **74**, 1880 (1999).
[6] T. Rasing, Appl. Phys. B: Lasers Opt. **68**, 477 (1999).
[7] R. Vollmer, Q.Y. Jin, H. Regensburger, and J. Kirschner, J. Magn. Magn. Mater. **199**, 611 (1999).
[8] T.V. Murzina, E.A. Ganshina, S.V. Guschin, T.V. Misuryaev, and O.A. Aktsipetrov, Appl. Phys. Lett. **73**, 3769 (1998).
[9] R. Carey, D.M. Newman, and M.L. Wears, Phys. Rev. B **58**, 14 175 (1998).
[10] D. Budker, V. Yashchuk, and M. Zolotorev, Phys. Rev. Lett. **81**, 5788 (1998).
[11] M. Straub, R. Vollmer, and J. Kirschner, Phys. Rev. Lett. **77**, 743 (1996).
[12] T. Rasing, in *Notions and Perspectives of Nonlinear Optics*, edited by O. Keller (World Scientific, Singapore, 1996), pp. 339–369.
[13] T. Rasing, M.G. Koerkamp, B. Koopmans, and H. van der Berg, J. Appl. Phys. **79**, 6181 (1996).
[14] J. Reif, C. Rau, and E. Matthias, Phys. Rev. Lett. **71**, 1931 (1993).
[15] G.S. Agarwal, P.A. Lakshmi, J.P. Connerade, and S. West, J. Phys. B **30**, 5971 (1997).
[16] *Nonlinear Optics in Metals*, edited by K. H. Bennemann (Oxford University Press, Oxford, 1998).
[17] A.K. Zvezdin and N.F. Kubrakov, JETP **89**, 77 (1999).
[18] V.M. Arutunyan, G.G. Adonts, E.G. Kanetsian, and S.T. Hovsepian, Opt. Appl. **27**, 151 (1997).
[19] A.V. Petukhov, I.L. Lyubchanskii, and T. Rasing, Phys. Rev. B **56**, 2680 (1997).
[20] A.K. Zvezdin, Physica A **241**, 444 (1997).
[21] U. Pustogowa, W. Hübner, K.H. Bennemann, and T. Kraft, Z. Phys. B: Condens. Matter **102**, 109 (1997).
[22] A. Dähn, W. Hübner, and K.H. Bennemann, Phys. Rev. Lett. **77**, 3929 (1996).
[23] U. Pustogowa, T.A. Luce, W. Hübner, and K.H. Bennemann, J. Appl. Phys. **79**, 6177 (1996).
[24] W. Hübner, Phys. Rev. B **42**, 11 553 (1990).
[25] J. E. Sipe and G. I. Stegeman, in *Surface Polaritons*, edited by V. M. Agranovich and D. L. Mills (North-Holland, Amsterdam, 1982), pp. 661–701.
[26] P. Guyot-Sionnest, W. Chen, and Y.R. Shen, Phys. Rev. B **33**, 8254 (1986).
[27] G.L. Richmond, J.M. Robinson, and V.L. Shannon, Prog. Surf. Sci. **28**, 1 (1988).
[28] R. Bavli and Y.B. Band, Phys. Rev. A **43**, 5044 (1991).
[29] T. F. Heinz, in *Nonlinear Surface Electromagnetic Phenomena*, edited by H.-E. Ponath and G. I. Stegeman (Elsevier, Amsterdam, 1991), pp. 353–416.
[30] S. Janz and H.M. van Driel, Int. J. Nonlinear Opt. Phys. **2**, 1 (1993).
[31] G. A. Reider and T. F. Heinz, in *Photonic Probes of Surfaces*, edited by P. Halevi (North-Holland, Amsterdam, 1995), pp. 413–478.
[32] A. Liebsch, in *Photonic Probes of Surfaces*, edited by P. Halevi (North-Holland, Amsterdam, 1995), pp. 479–532.
[33] K. Pedersen, in *Studies in Classical and Quantum Nonlinear Phenomena*, edited by O. Keller (Nova Science, New York, 1995), pp. 385–418.
[34] J.F. McGilp, J. Phys. D **29**, 1812 (1996).
[35] A. Liebsch, *Electronic Excitations at Metal Surfaces* (Plenum, New York, 1997).
[36] V.M. Axt and S. Mukamel, Rev. Mod. Phys. **70**, 145 (1998).
[37] A. Liu and G.W. Bryant, Phys. Rev. B **59**, 2245 (1999).
[38] J.P. Dewitz, J. Chen, and W. Hübner, Phys. Rev. B **58**, 5093 (1998).
[39] J.P. Dewitz and W. Hübner, Appl. Phys. B: Lasers Opt. **68**, 491 (1999).

[40] T. Asada and S. Blügel, Phys. Rev. Lett. **79**, 507 (1997).
[41] A.V. Petukhov and A. Liebsch, Surf. Sci. **294**, 381 (1993).
[42] A.V. Petukhov and A. Liebsch, Surf. Sci. **320**, L51 (1994).
[43] A.V. Petukhov and A. Liebsch, Surf. Sci. **331–333**, 1335 (1995).
[44] A.V. Petukhov and A. Liebsch, Surf. Sci. **334**, 195 (1995).
[45] H. Ishida, A.V. Petukhov, and A. Liebsch, Surf. Sci. **340**, 1 (1995).
[46] M. Kuchler and F. Rebentrost, Phys. Rev. Lett. **71**, 2662 (1993).
[47] M. Kuchler and F. Rebentrost, Phys. Rev. B **50**, 5651 (1994).
[48] F. Rebentrost, Prog. Surf. Sci. **48**, 71 (1995).
[49] N.D. Lang and A.R. Williams, Phys. Rev. B **18**, 616 (1978).
[50] A. Zangwill and P. Soven, Phys. Rev. A **21**, 1561 (1980).
[51] M.J. Stott and E. Zaremba, Phys. Rev. A **21**, 12 (1980).
[52] G.D. Mahan, Phys. Rev. A **22**, 1780 (1980).
[53] E. Runge and E.K.U. Gross, Phys. Rev. Lett. **52**, 997 (1984).
[54] M. Weber and A. Liebsch, Phys. Rev. B **35**, 7411 (1987); **37**, 1019(E) (1988).
[55] A. Liebsch, Phys. Rev. Lett. **61**, 1233 (1988); **61**, 1897(E) (1988).
[56] A. Liebsch and W.L. Schaich, Phys. Rev. B **40**, 5401 (1989).
[57] H. Ishida and A. Liebsch, Phys. Rev. B **50**, 4834 (1994).
[58] A. Liebsch, Appl. Phys. B: Lasers Opt. **68**, 301 (1999).
[59] A. Liebsch, Phys. Rev. B **40**, 3421 (1989).
[60] P. Guyot-Sionnest and Y.R. Shen, Phys. Rev. B **35**, 4420 (1987).
[61] P. Guyot-Sionnest and Y.R. Shen, Phys. Rev. B **38**, 7985 (1988).
[62] P. Guyot-Sionnest, A. Tadjeddine, and A. Liebsch, Phys. Rev. Lett. **64**, 1678 (1990).
[63] R. Vollmer, M. Straub, and J. Kirschner, Surf. Sci. **352–354**, 684 (1996).
[64] R. Vollmer, M. Straub, and J. Kirschner, Surf. Sci. **352–354**, 937 (1996).
[65] G. Spierings, V. Koutsos, H.A. Wierenga, M.W.J. Prins, D. Abraham, and T. Rasing, J. Magn. Magn. Mater. **121**, 109 (1993).
[66] G. Spierings, V. Koutsos, H.A. Wierenga, M.W.J. Prins, D. Abraham, and T. Rasing, Surf. Sci. **287–288**, 747 (1993).
[67] P. Blaha, K. Schwarz, and J. Luitz, *WIEN97, A Full Potential Linearized Augmented Plane Wave Package for Calculating Crystal Properties* (Karlheinz Schwarz, Vienna, 1999).
[68] J.E. Sipe, D.J. Moss, and H.M. van Driel, Phys. Rev. B **35**, 1129 (1987).
[69] O. Keller, Phys. Rep. **268**, 85 (1996).
[70] T. Rasing, Appl. Phys. A: Solids Surf. **59**, 531 (1994).
[71] H.A. Wierenga, M.W.J. Prins, D.L. Abraham, and T. Rasing, Phys. Rev. B **50**, 1282 (1994).
[72] T.A. Luce, W. Hübner, A. Kirilyuk, T. Rasing, and K.H. Bennemann, Phys. Rev. B **57**, 7377 (1998).
[73] A. Liebsch and W.L. Schaich, Phys. Rev. B **52**, 14219 (1995).
[74] U. Pustogowa, Ph.D. thesis, Freie Universität Berlin, Berlin, 1994.
[75] J. P. Dewitz, Ph.D. thesis, Martin-Luther-Universität Halle-Wittenberg, Halle, 1999.
[76] W. Hübner, in *Nonlinear Optics in Metals*, edited by K. H. Bennemann (Oxford University Press, Oxford, 1998), pp. 268–436.
[77] H. Haug and S. Schmitt-Rink, Prog. Quantum Electron. **9**, 3 (1984).
[78] D. Misemer, J. Appl. Phys. **61**, 3355 (1987).
[79] D.K. Misemer, J. Magn. Magn. Mater. **72**, 267 (1988).
[80] H. Haug and S. Schmitt-Rink, J. Opt. Soc. Am. B **2**, 1135 (1985).
[81] C. Aversa and J.E. Sipe, Phys. Rev. B **52**, 14 636 (1995).
[82] J.E. Sipe and E. Ghahramani, Phys. Rev. B **48**, 11 705 (1993).
[83] W. Hübner, K.H. Bennemann, and K. Böhmer, Phys. Rev. B **50**, 17 597 (1994).
[84] H. Poincaré, *Théorie Mathématique de la Lumière* (Gauthiers-Villars, Paris, 1892).
[85] R. M. A. Azzam and N. M. Bashara, *Ellipsometry and Polarized Light* (North-Holland, Amsterdam, 1987).
[86] M. A. M. Groot Koerkamp, M. S. thesis, K. U. Nijmegen, Nijmegen, 1995.
[87] J. Thomassen, F. May, B. Feldmann, M. Wuttig, and H. Ibach, Phys. Rev. Lett. **69**, 3831 (1992).
[88] D. J. Singh, *Planewaves, Pseudopotentials and the LAPW Method* (Kluwer, Boston, 1994).
[89] J.P. Perdew, K. Burke, and M. Ernzerhof, Phys. Rev. Lett. **77**, 3865 (1996); **78**, 1396(E) (1997).
[90] P.E. Blöchl, O. Jepsen, and O.K. Andersen, Phys. Rev. B **49**, 16 223 (1994).
[91] J. Kuneš, P. Novak, R. Schmid, P. Blaha, and K. Schwarz, Phys. Rev. B **64**, 153102 (2001).
[92] L. Nordström, J.M. Wills, P.H. Andersson, P. Söderlind, and O. Eriksson, Phys. Rev. B **63**, 035103 (2001).
[93] F. Wilhelm, P. Srivastava, H. Wende, A. Ney, N. Haack, G. Ceballos, M. Farle, and K. Baberschke, J. Synchrotron Radiat. **6**, 699 (1999).
[94] H. Wende, P. Srivastava, D. Arvanitis, F. Wilhelm, L. Lemke, A. Ankudinov, J.J. Rehr, J.W. Freeland, Y.U. Idzerda, and K. Baberschke, J. Synchrotron Radiat. **6**, 696 (1999).
[95] R. Courths and S. Hüfner, Phys. Rep. **112**, 53 (1984).
[96] J.A. Knapp, F.J. Himpsel, and D.E. Eastman, Phys. Rev. B **19**, 4952 (1979).
[97] A. Marini, G. Onida, and R. Del Sole, Phys. Rev. B **64**, 195125 (2001).
[98] H. Petek and S. Ogawa, Prog. Surf. Sci. **56**, 239 (1997).
[99] R. Vollmer, in *Nonlinear Optics in Metals*, edited by K. H. Bennemann (Oxford University Press, Oxford, 1998), pp. 42–131.
[100] X. Qian, F. Wagner, M. Petersen, and W. Hübner, J. Magn. Magn. Mater. **213**, 12 (2000).
[101] X. Qian and W. Hübner, Phys. Rev. B **60**, 16 192 (1999).
[102] H.A. Wierenga, W. de Jong, M.W.J. Prins, T. Rasing, R. Vollmer, A. Kirilyuk, H. Schwabe, and J. Kirschner, Phys. Rev. Lett. **74**, 1462 (1995).
[103] Y. Suzuki, T. Katayama, P. Bruno, S. Yuasa, and E. Tamura, Phys. Rev. Lett. **80**, 5200 (1998).
[104] R. Megy, A. Bounouh, Y. Suzuki, P. Beauvillain, P. Bruno, C. Chappert, B. Lecuyer, and P. Veillet, Phys. Rev. B **51**, 5586 (1995).
[105] Y.Z. Wu, R. Vollmer, H. Regensburger, X.-F. Jin, and J. Kirschner, Phys. Rev. B **63**, 054401 (2000).
[106] P.J. Feibelman, Prog. Surf. Sci. **12**, 287 (1982).
[107] T. Katayama, Y. Suzuki, H. Awano, Y. Nishihara, and N. Koshizuka, Phys. Rev. Lett. **60**, 1426 (1988).
[108] D. W. Lynch and W. R. Hunter, in *Handbook of Optical Constants in Solids*, edited by E. D. Palik (Academic Press, London, 1985), pp. 275–367.
[109] G. Petrocelli, S. Martellucci, and R. Francini, Appl. Phys. A: Solids Surf. **56**, 263 (1993).
[110] K. Böhmer, Ph.D. thesis, Freie Universität Berlin, Berlin, 1994.